

Molecular descriptors suggest stapling as a strategy for optimizing membrane permeability of cyclic peptides

Cite as: J. Chem. Phys. **156**, 065101 (2022); <https://doi.org/10.1063/5.0078025>

Submitted: 09 November 2021 • Accepted: 20 January 2022 • Accepted Manuscript Online: 20 January 2022 • Published Online: 08 February 2022

 Jianguo Li, Srinivasaraghavan Kannan, Pietro Aronica, et al.



[View Online](#)



[Export Citation](#)



[CrossMark](#)

ARTICLES YOU MAY BE INTERESTED IN

[Impact of confinement and polarizability on dynamics of ionic liquids](#)

The Journal of Chemical Physics **156**, 064703 (2022); <https://doi.org/10.1063/5.0077408>

[Critical assessment of machine-learned repulsive potentials for the density functional based tight-binding method: A case study for pure silicon](#)

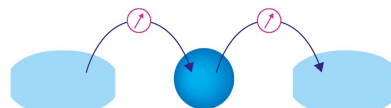
The Journal of Chemical Physics **156**, 064101 (2022); <https://doi.org/10.1063/5.0081159>

[Evaluating quantum alchemy of atoms with thermodynamic cycles: Beyond ground electronic states](#)

The Journal of Chemical Physics **156**, 064106 (2022); <https://doi.org/10.1063/5.0079483>

Webinar

[Interfaces: how they make or break a nanodevice](#)



March 29th – Register now

 Zurich
Instruments

Molecular descriptors suggest stapling as a strategy for optimizing membrane permeability of cyclic peptides

Cite as: J. Chem. Phys. 156, 065101 (2022); doi: 10.1063/5.0078025

Submitted: 9 November 2021 • Accepted: 20 January 2022 •

Published Online: 8 February 2022



View Online



Export Citation



CrossMark

Jianguo Li,^{1,2,a)} Srinivasaraghavan Kannan,¹ Pietro Aronica,¹ Christopher J. Brown,³ Anthony W. Partridge,⁴ and Chandra S. Verma^{1,5,6,a)}

AFFILIATIONS

¹ Bioinformatics Institute, A*STAR, 30 Biopolis Street, Matrix, Singapore 138671

² Singapore Eye Research Institute, Singapore 169856, Singapore

³ p53 Laboratory (A-STAR), 8A Biomedical Grove, Immunos, 138648, Singapore

⁴ MSD International, Translation Medicine Research Centre, 8 Biomedical Grove, #04-01/05 Neuros Building, Singapore 138665, Singapore

⁵ Department of Biological Sciences, National University of Singapore, 117543, Singapore

⁶ School of Biological Sciences, Nanyang Technological University, 637551, Singapore

^{a)} Authors to whom correspondence should be addressed: lijg@bii.a-star.edu.sg and Chandra@bii.a-star.edu.sg

ABSTRACT

Cyclic peptides represent a promising class of drug candidates. A significant obstacle limiting their development as therapeutics is the lack of an ability to predict their membrane permeability. We use molecular dynamics simulations to assess the ability of a set of widely used parameters in describing the membrane permeability of a set of model cyclic peptides; the parameters include polar surface area (PSA), the number of hydrogen bonds, and transfer free energy between an aqueous phase and a membrane mimicking phase. These parameters were found to generally correlate with the membrane permeability of the set of cyclic peptides. We propose two new descriptors, the charge reweighted PSA and the non-polar surface area to PSA ratio; both show enhanced correlation with membrane permeability. This inspired us to explore crosslinking of the peptide to reduce the accessible surface area of the backbone polar atoms, and we find that this can indeed result in reductions in the accessible PSA. This gives reason to speculate that crosslinking may result in increased permeability, thus suggesting a new scaffold for the development of cyclic peptides as potential therapeutics.

Published under an exclusive license by AIP Publishing. <https://doi.org/10.1063/5.0078025>

I. INTRODUCTION

Cyclic peptides are useful drug scaffolds because of properties such as tunable chemical linkers, long half-lives, and high efficiency in disrupting protein–protein interfaces.^{1,2} However, their development as drugs has been limited by cell permeability issues.^{1,3} Although several natural and synthetic cyclic peptides have been approved by the Food and Drug Administration (FDA),^{4,5} there are few rational principles to guide the design of membrane permeable cyclic peptides. Compared to small molecules, cyclic peptides are endowed with large numbers of chiral atoms, which not only affects binding to receptors but also significantly modulates their

membrane permeability.^{6–8} For small molecules, the membrane permeability can be adjusted by varying the solvent accessible polar surface area (PSA). PSA is defined as the sum of the solvent accessible surface area (SASA) of all polar atoms, such as backbone carbonyl, oxygen, and nitrogen and their bonded hydrogen atoms, which can be calculated by rolling a solvent probe along the surface of the molecule.⁹ However, cyclic peptides are usually flexible and display ensembles of diverse conformations. This can result in conformational transitions when partitioning from the aqueous phase to the membrane phase,^{10,11} which is an additional layer of complexity when rationalizing their membrane permeation. Understanding the mechanism of membrane permeation and development of new

metrics that can predict membrane permeability holds the potential to accelerate the development of new cyclic peptide drugs.

The membrane permeability of a solute can be described by the inhomogeneous solubility-diffusion model.^{12–14} In a bilayer membrane model, the membrane permeability coefficient P_m of a molecule can be calculated using the following equation:

$$R = \frac{1}{P_m} = \int_{r_2}^{r_1} \frac{\exp[-\Delta G/kT]}{D(r)} dr \approx \frac{1}{D} \int_{r_2}^{r_1} \exp[-\Delta G(r)/kT] dr, \quad (1)$$

where r is the reaction coordinate, which is usually chosen as the distance between the center of mass of the molecule and the center of mass of the membrane along the membrane normal; D is the local diffusivity at r , and ΔG is the transfer free energy or the potential of mean force (PMF) between the aqueous phase and the membrane phase, which can be calculated from molecular dynamics (MD) simulations. Although the exact membrane permeability can be accurately calculated, in practice, it is successful only for a few small molecule or short peptide drugs that passively diffuse across the membrane^{14–16} and remains a big challenge for most of the peptide molecules due to insufficient sampling of the conformational space.¹⁷ Recently, Sugita *et al.*¹⁶ have made a breakthrough by calculating the membrane permeability of 156 cyclic peptides using replica exchange umbrella sampling molecular dynamics simulations and found a reasonable correlation between the experimental determined membrane permeability and the *in silico* predictions. Their simulations also revealed that the rate limiting step for most peptides translocation across the membrane is to cross the bilayer center. However, these calculations are computationally intensive. The problem becomes a little more tractable for a family of peptides that are homologous to each other. For example, for a given class of structurally similar cyclic peptides, if we assume that the diffusion coefficients of the cyclic peptides are similar, the membrane permeability can be ranked by the integration of ΔG along the translocation pathway [Eq. (1)]. If we further assume that the shape of the PMF is similar among these peptides, one can use the free energy differences ΔG between the aqueous phase and the membrane phase to rank their membrane permeabilities. For example, Dickson *et al.* used the partition free energy to predict the membrane permeability of 49 drug molecules.¹⁸ For larger molecules, such as peptides, the calculation of ΔG often suffers from lack of convergence and hence requires advanced sampling methods.¹⁶ In the case of peptides, the biphasic model, consisting of an aqueous phase and a membrane mimicking phase, has been used due to its simplicity.^{19,20} Using grid inhomogeneous solvation theory (GIST), Kamenik *et al.* found that the free energy differences between a set of cyclic peptides from the aqueous phase to the chloroform phase correlated very well with the experimentally reported membrane permeability, with the coefficient of determination $R^2 = 0.846$.²¹

Since the accurate computation of free energies is not a trivial task, various studies have focused on searching for empirical parameters that can easily be computed and that correlate with membrane permeability.^{22–24} According to the mechanism of passive diffusion, membrane permeability depends on the solvation free energy differences between the two media and is correlated with

the PSA, the molecular size, and the overall hydrophobicity of a molecule. For relatively rigid small molecules, the PSA is almost constant along the entire translocation pathway, but the PSA of peptides can fluctuate significantly due to their high inherent flexibility, and hence requires efficient sampling of their conformational spaces.²⁵ It has been proposed that PSA less than 1.4 nm^2 in non-polar medium is necessary for membrane permeable macrocycles;^{26,27} nevertheless, challenges such as force field accuracy and sampling remain.²⁸ For example, using multicanonical molecular dynamics simulations, Ono *et al.*²⁰ found that the average PSA in either water or in a membrane mimicking medium correlates poorly with the membrane permeability of a set of cyclic hexapeptides. However, they found that the average total solvent accessible surface area (SASA) in cyclohexane correlated well with membrane permeability, and yet it did not do so when the membrane mimic used was chloroform.

In this study, we use molecular dynamics (MD) simulations to evaluate the correlations of various molecular parameters with the reported experimental membrane permeabilities of a set of nine cyclic hexapeptides.⁷ These peptides share the same sequence and differ only in the chirality of individual residues. We employ a simple biphasic model to mimic the membrane system and test the correlations of several molecular descriptors of the peptides with the membrane permeability of the peptides, e.g., the transfer free energy from aqueous phase to a membrane mimicking phase ΔG , the intra-peptide hydrogen bonds (HBs), and surface parameters, such as PSA.

II. METHODS

The peptides were taken from the work of Rezai *et al.*⁷ and are all based on the template sequence of cyclo[Leu-Leu-Leu-Leu-Pro-Tyr], differing only in the chirality of individual residues (Table I). Rezai *et al.* used a parallel artificial membrane permeability assay (PAMPA) to determine the membrane permeability of the peptides.^{7,29,30} The apparent permeability coefficient P_m of the peptides was calculated by normalizing the steady state flux of the peptide across the PAMPA membrane by the surface area of the membrane and the initial concentration of the peptide.^{29,31} In our study, the calculations of the transfer free energies of the peptides from the aqueous to the membrane mimicking phase (e.g., hexane) and the properties of the peptides in hexane, chloroform, and octanol solutions were carried out using the AMBER14SB force field, which has been shown to be quite robust in modeling cyclic peptides.^{32,33} The parameters for the linker groups used for crosslinking the peptides (Table II) were taken from our previous study.³⁴ Restrained electrostatic potential (RESP) charges were assigned to the non-natural amino acids using a protocol based on the parameterization of natural amino acids.^{35,36} The OAB residue is an unnatural amino acid in one of our controls, Romidepsin (ROM), whose side chain contains two carbon and one double bond between the beta carbon and alpha carbon. It was parameterized using NWChem,³⁷ while the RED server³⁸ was used for the other residues; the Hartree-Fock method using the 6-31g* basis set was used. The antechamber module in AMBER18³⁹ was used to assign atom types,⁴⁰ and the AMBER14SB force field was used,⁴¹ with the TIP3P model of water.⁴² The topologies of the cyclic peptides were built using the leap module of the AMBER18 package. The parameters for chloroform and octanol were obtained

TABLE I. The sequence, the number of intra-peptide hydrogen bonds (HB), and permeability of the cyclic peptides.

Peptide ^a	Sequence	Intra-peptide HB (water) ^b	Intra-peptide HB (hexane) ^b	$\log P_m$ ^a
1	dL-dL-L-dL-P-Y	0.26	2.9	-6.2
2	dL-dL-dL-dL-P-Y	1.08	3.23	-7
3	L-L-L-dL-P-Y	0.71	3.36	-7.1
4	L-dL-dL-dL-P-Y	1.06	2.98	-7.2
5	L-L-L-L-dP-Y	1.01	2.35	-7.3
6	dL-dL-dL-dL-dP-Y	1.77	2.72	-7.3
7	L-L-dL-dL-P-Y	1.53	2.94	-7.3
8	L-dL-L-dL-dP-Y	0.26	2.53	<=-8.1
9	L-dL-L-L-dP-Y	1.61	1.53	<=-8.1

^aThe peptide sequence and the experimental permeability were taken from the work of Rezai *et al.*⁷ The permeability coefficient $\log P_m$ was determined using PAMPA.

^bThe number of intra-peptide hydrogen bonds (HB) of the peptides in water and hexane were calculated from our MD simulations.

TABLE II. Simulated parameters of the crosslinked cyclic peptides.

Peptide	Sequence ^a	HB_{pp}^H ^b	HB_{pw}^W ^c	PSA^H ^d	$cPSA^H$	NSA/PSA^H	$NSA/cPSA^H$	ΔPSA^{H-W} ^e	$\Delta cPSA^{H-W}$	$\Delta NSA/cPSA^{H-W}$
ROM	RCR-VAL-dCYS-OAB-VAL	1.52	7.22	1.01	0.55	5.06	9.38	-0.13	-0.07	1.39
ROH	RCR-VAL-dCYS-OAB-VAL	1.32	7.85	1.08	0.58	4.91	9.21	-0.04	0	-0.18
ROM1M	RCM-VAL-dCYS-OAB-VAL	1.27	8.43	1.1	0.62	4.71	8.38	-0.09	-0.05	0.66
ROMs1	dMKC-VAL-dOEC-OAB-VAL	1.58	7.98	0.94	0.52	6.33	11.45	0.06	0.04	-0.78
ROMs2	dMKC-VAL-dMKC-OAB-VAL	1.16	6.79	1.05	0.59	5.04	8.99	0.152	0.09	-1.85
Pep8	LEU-dLEU-LEU-dLEU-dPRO-TYR	2.53	13.94	1.57	0.88	4.53	8.1	-0.17	-0.05	0.18
pep8cys	CYS-dLEU-LEU-dCYS-dPRO-TYR	1.15	11.7	1.66	0.91	3.61	6.62	-0.11	-0.06	0.47
pep8s1	MKC-dLEU-LEU-dOEC-dPRO-TYR	2.47	10.9	1.27	0.7	5.78	10.43	-0.08	-0.02	0.09
pep8s2	MKC-dLEU-LEU-dMKC-dP-TYR	1.6	10.0	1.36	0.74	4.98	9.07	-0.016	-0.01	0.22
Pep9	LEU-dLEU-LEU-LEU-dPRO-TYR	1.53	10.9	1.59	0.88	4.38	7.93	0.016	0.03	-0.37
pep9cys	CYS-dLEU-LEU-CYS-dPRO-TYR	0.18	12.0	1.8	0.96	3.37	6.23	0.038	0.02	-0.03
pep9s1	MKC-dLEU-LEU-dOEC-dPRO-TYR	2.86	10.2	1.2	0.66	5.78	10.46	-0.238	-0.13	1.77
pep9s2	MKC-dLEU-LEU-dMKC-dPRO-TYR	1.88	11.3	1.33	0.74	4.82	8.69	-0.11	-0.04	-0.08

^aMKC and OEC are residues at the stapling sites, with 4 and 7 carbon sidechains, respectively; RCR and OAB are the two unnatural residues in romidepsin; RCM is an RCR analog with one extra carbon in the linker.

^b HB_{pp}^H is the number of intra-peptide hydrogen bonds in hexane; superscript H indicates simulation in hexane, while subscript pp indicates the number of intra-peptide hydrogen bonds.

^c HB_{pw}^W is the number of hydrogen bonds in water; superscript W denotes simulation in water, and subscript pw denotes the number of hydrogen bonds between peptide and water.

^dSuperscript H denotes the surface parameters of the peptide in hexane.

^eSuperscript H-W denotes the differences in the surface parameters of the peptide between the hexane phase (H) and the water phase (W), e.g., $\Delta PSA^{H-W} = PSA^H - PSA^W$; $\Delta cPSA^{H-W} = cPSA^H - cPSA^W$; and $\Delta NSA/cPSA^{H-W} = NSA/cPSA^H - NSA/cPSA^W$.

from the group of van der Spoel (<http://virtualchemistry.org>).⁴³ Peptides can display different protonation states at different pH and in different microenvironments,^{44,45} however, the peptides used in this study only consist of cyclic backbones and the side chains of Leu, Pro, and Tyr, and they do not contain titratable groups (the pKa of the sidechain of Tyr is ~10.1 and hence will remain protonated under the conditions explored here); hence, we used the same force field parameters corresponding to physiological pH in both aqueous solution and the membrane mimicking environment.

To understand how the peptide partitions into the membrane, we constructed a biphasic system consisting of one organic slab and

one aqueous phase; the former is a mimic of a membrane and can be described using hexane, chloroform, or octanol.^{14,46} The details of the system setup are given in Table S1. We used umbrella sampling simulations to calculate the transfer free energies of the peptides from the aqueous phase to the organic phase. In each umbrella sampling simulation, the z-position was chosen as the reaction coordinate, which is the position of the center of mass of the peptide with respect to the center of mass of the hexane slab along the slab normal (z-direction), and the path is described by 24 equally spaced windows with 0.15 nm between adjacent windows, which are sufficient to achieve the overlap of the distributions of the potential energy between adjacent windows. Each window was simulated for 50 ns

with a harmonic potential of 1000 kJ/mol/nm to restrain the peptide to a specified z-position. The last 30 ns were used to construct the PMF as a function of the z-position using the weighted histogram analysis method (WHAM).⁴⁷

To explore whether the differences in solubilities of the peptides between water and the organic phases (membrane mimics) could be correlated with membrane permeability, we also simulated each peptide in water and the membrane mimicking medium (we explored hexane, chloroform, and octanol separately) for 400 ns each, using the last 300 ns (as the system had equilibrated, see later) for analysis. Compared to the time taken to compute the PMF in the biphasic system, the simulation of the peptide in an organic medium is about one order of magnitude faster due to the smaller size of the simulation box and without the need to simulate the intermediate states along the translocation pathway. The solubility of the peptide was estimated by computing the solvent accessible surface area (SASA) using the double cubic lattice method (DCLM) that is implemented in the GROMACS package.⁴⁸ SASA is the surface formed by rolling a solvent probe (e.g., water molecule) along the van der Waals surface of the peptide molecule.⁴⁹ In this study, the probe radius was chosen as 1.4 nm. The SASA was then further decomposed into PSA and non-polar surface area (NSA). For the peptides used in this study, the polar atoms refer to the CO and NH groups of the backbone as well as the OH group of the Tyr sidechain, and all other atoms are treated as non-polar atoms. The PSA of the peptide was calculated by summing the atomic area of the polar atoms (e.g., the CO and NH groups in the backbone and the OH groups in the side chains of Tyr residues), and NSA was calculated by the subtraction of the PSA from SASA. The charge weighted PSA (cPSA) was calculated using $\sum q_i^* PSA_i$, where q_i is the partial atomic charge of the polar atoms and PSA_i is the atomic area of the individual polar atoms. The above simulations revealed that hexane is a better mimic of the lipid tails of the membrane, and so we carried out two additional sets of simulations in hexane using the CHARMM36⁵⁰ and CHARMM36M⁵¹ force fields to study the effects of force fields on the prediction of membrane permeability; the corresponding parameters were generated using CHARMM-GUI.^{52,53} In addition, we further explored the AMBER03 force field⁵⁴ because Ono *et al.* had shown that this force field yields a good correlation between simulations carried out in cyclohexane and experimental data.²⁰ Our results showed that exposure of the backbone polar atoms appears to modulate solubility, and hence, to examine this, we decided to explore these effects by introducing crosslinks to reduce the exposure of the backbone polar atoms. For this, we choose two poorly permeable peptides, pep8 and pep9 (Table I), and designed six crosslinked analogs with different lengths of the linkers, by crosslinking residues 1 and 4. These were called pep8cys and pep9cys, in which two cysteine residues were used via a disulfide bridge to crosslink the peptides; pep8s1 and pep9s1 in which the crosslinker consisted of 11 carbon atoms, and pep8s2 and pep9s2 in which the crosslinker consisted of eight carbon atoms (Table II). Each crosslinked cyclic peptide was subjected to 400 ns of simulations in both hexane and water. For comparison, we also performed simulations of a FDA approved drug that is known to be cell permeable, romidepsin (ROM). To examine the effect of crosslinking on peptide permeability, we also constructed and simulated two hydrocarbon stapled analogs of romidepsin: ROMs1 (11 carbon crosslinker) and ROMs2 (8 carbon crosslinker); as a further control, we explored the effects of removing the geometrical

constraints in romidepsin by reducing the disulfide bridge (ROH). Details of the system setup are given in Table S2.

In all the simulations, the bonds between the hydrogen atoms and any heavy atoms were constrained using the LINCS algorithm, enabling a time step of 2 fs to be used.⁵⁵ Both Lennard-Jones interactions and short-range electrostatic interactions were cut at 1.0 nm, and long-range electrostatic interactions were calculated using PME.⁵⁶ All simulations were performed in the NPT ensemble, with temperature and pressure being maintained at 300 K and 1 bar using the Nosé–Hoover thermostat and the Parrinello–Rahman barostat, respectively. The hydrogen bond is identified when the distance between the donor atom and the acceptor atom is smaller than 0.35 nm, and the angle subtended by the donor–hydrogen–acceptor atoms is smaller than 30°. Simulations were carried out using GROMACS 5.1.⁵⁷ Surface parameters (e.g., PSA, NSA, and SASA) were calculated using the g_sas command in GROMACS with a probe radius of 1.4 nm; RMSD of the peptides was calculated using the g_rms command in GROMACS, and the number of hydrogen bonds were calculated using the g_hbond command in GROMACS; cPSA was calculated using our own python script. Principle component analysis (PCA) was carried out using the GROMACS commands g_covar and g_anaeig, and the probability distribution of the conformational states along the first two principle components PC1 and PC2 was calculated using our own code; PMF was constructed using the GROMACS command g_wham.

III. RESULTS AND DISCUSSIONS

A. Correlation of transfer free energy with permeability

We first examined the transfer free energy of the peptides from water to hexane (the potential of mean force, PMF, Figs. 1 and S1). All the peptides displayed a free energy minimum at the water–hexane interface, where the non-polar atoms of the peptide undergo desolvation, while the polar atoms are still solvated with water molecules, as shown by the snapshots in Fig. S2. At the hexane–water interface, most Leu residues prefer to penetrate into the hexane phase, while the Tyr side chain is largely solvated with water molecules. This is consistent with computational studies that have reported that free energy of transfer from water to a bilayer center is negative for Leu, but slightly positive for Tyr, and contrasts with the negative free energies for the other aromatic sidechains Phe and Trp.⁵⁸ As the peptides further penetrate into the hexane phase, the polar atoms start to desolvate, resulting in an increase in the PMF. In the case of a membrane, the free energy barrier associated with polar groups, particularly the charged groups, exists mainly in the lipid tail region of the membrane, where the polar atoms get desolvated.^{58,59} This suggests that the free energy difference between the water phase and an organic phase mimicking the lipid tail region of the membrane ΔG could be a useful parameter to assess membrane permeability. We find that the calculated ΔG between the aqueous phase and the hexane phase generally correlates reasonably with the experimental permeability, with the calculated coefficient of determination $R^2 = 0.613$ [Fig. 1(b)].

The ΔG of small molecules can be estimated through the use of simple empirical methods, such as group contribution theory.⁶⁰ In contrast, calculation of the ΔG for peptides, particularly for peptide enantiomers, requires rigorous sampling of the conformational

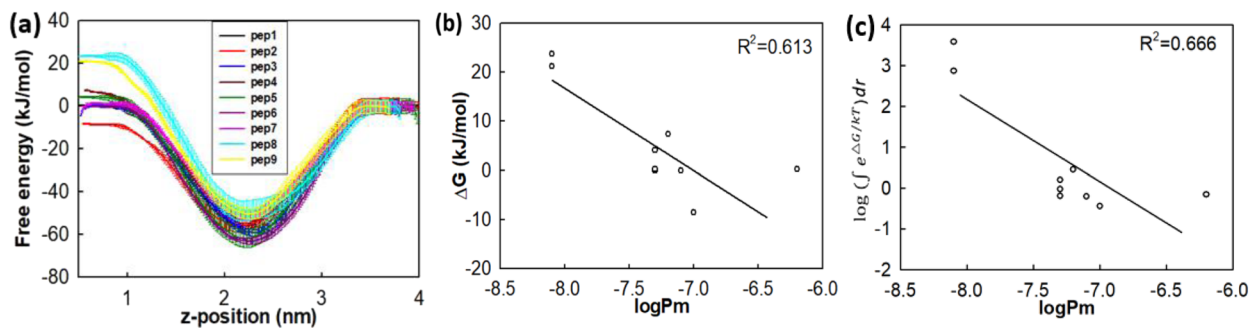


FIG. 1. Transfer free energy from aqueous phase to hexane. (a) Potential of mean force for the peptide transferring from water to hexane as a function of the z-position of the peptide with respect to the center of mass of the hexane slab; (b) correlation of the free energy difference with the peptide permeability; and (c) correlation of the integration of the potential of mean force based on Eq. (1) with the peptide permeability.

spaces because a peptide, in contrast to small molecules that largely are relatively rigid, is very flexible and is characterized by a complex free energy landscape with many metastable states separated by free energy barriers.^{61,62} We wondered whether the free energies of the intermediate states along the pathway across the hexane–water biphasic system could be used to recapitulate the experimentally observed the membrane permeabilities of the peptide enantiomers. From Eq. (1), we know that the membrane permeability not only depends on the free energy difference ΔG but also depends on the diffusion coefficient along the translocation pathway. As the peptides in this study only differ in chirality, we can assume that their diffusion coefficients are similar. This allows us to integrate based on Eq. (1), and we find that although the membrane is modeled using a simple hexane–water biphasic system, integration of the free energies does result in a small improvement in correlation ($R^2 = 0.666$) [Fig. 1(c)]; however, these correlations are not very satisfactory.

B. Polar surface area in a membrane mimicking environment

Next, we looked for correlations between the exposed surface areas in both water and hexane with permeabilities of the peptides. The 400 ns simulations were found to have attained equilibrium rapidly in the properties of interest (Figs. S3 and S4). The overlap in the distribution of PSA in hexane between the different peptides (Fig. S4) suggests the necessity of using the ensemble averaged PSA from MD simulations instead of the PSA of a single conformation. Figure 2(a) shows a similar correlation as above between the ensemble averaged PSA in hexane and the peptide permeability ($R^2 = 0.624$). In contrast, the PSA in water shows poor correlation with the peptide permeability ($R^2 = 0.017$), suggesting that PSA in a membrane mimicking medium could possibly be a useful descriptor for the membrane permeability of such cyclic peptides. There is also poor correlation for the averaged total solvent accessible surface area (SASA) in either water or hexane [Fig. 2(b)]. This is in contrast to the computational study of Ono *et al.*,²⁰ in which the authors found a strong correlation between the total SASA in cyclohexane and the experimental permeability of eight cyclic peptide enantiomers ($R^2 = 0.872$). Interestingly, Ono *et al.* did not find any correlation of PSA in either cyclohexane or water with permeability ($R^2 = 0.063$).

Although the peptides used in the work of Ono *et al.* have the same amino acid content (e.g., four Leu residues, one Pro, and one Tyr) to the peptide used in this study, the sequences in the two studies are quite different, resulting in differences in the calculated PSA and SASA. For example, the PSA in our study ranges from 1.22 to 1.6 nm² [Fig. 2(a)], while the PSA in the work of Ono *et al.* spans a narrow range from 1.37 to 1.44 nm², suggesting that the peptides used in the study of Ono *et al.* are less flexible; this of course may also result from different solvents (cyclohexane) and force fields used in their study (AMBER03).

PSA is related to the desolvation free energy penalty associated with entry into the membrane, which is often balanced by the favorable free energy gain associated with the non-polar groups. To take into account the contribution from non-polar atoms, which provides the driving force for membrane penetration, we wondered if the ratio of non-polar surface area (NSA) to PSA would give a better correlation; indeed, we find that it does improve the correlation [$R^2 = 0.719$; Fig. 2(c)], suggesting that this ratio is a better descriptor for membrane permeability. As the NSA/PSA ratio considers both non-polar and polar groups of the peptide, it is also a more general parameter and is less dependent on the size of the peptide.

Although the NSA/PSA ratio appears to correlate better with membrane permeability compared to PSA alone, it still has some intrinsic limitations. PSA is defined by summing the atomic area of all polar atoms, such as oxygen and nitrogen, and does not account for the variations in partial atomic charges that characterize the atoms based on their environments. For example, COO⁻ has smaller PSA compared to COOH, but the former is associated with a higher free energy penalty during penetration into the membrane, resulting in discrepancy in the correlation of PSA with membrane permeability. To overcome this limitation, we propose a modified PSA, which reweights the atomic area of each polar atom with its partial atomic charge. The charge weighted PSA (cPSA) is calculated as $cPSA = \sum q_i * PSA_i$, where q_i is the partial atomic charge of the individual polar atom and PSA_i is the atomic area of the polar atom. When the PSA is weighted by the corresponding partial atomic charges, the correlations of cPSA and NSA/cPSA with membrane are increased (R^2 for cPSA is 0.668 compared to 0.624 for PSA; R^2 is 0.773 for NSA/cPSA compared to 0.719 for unweighted PSA, Fig. 3).

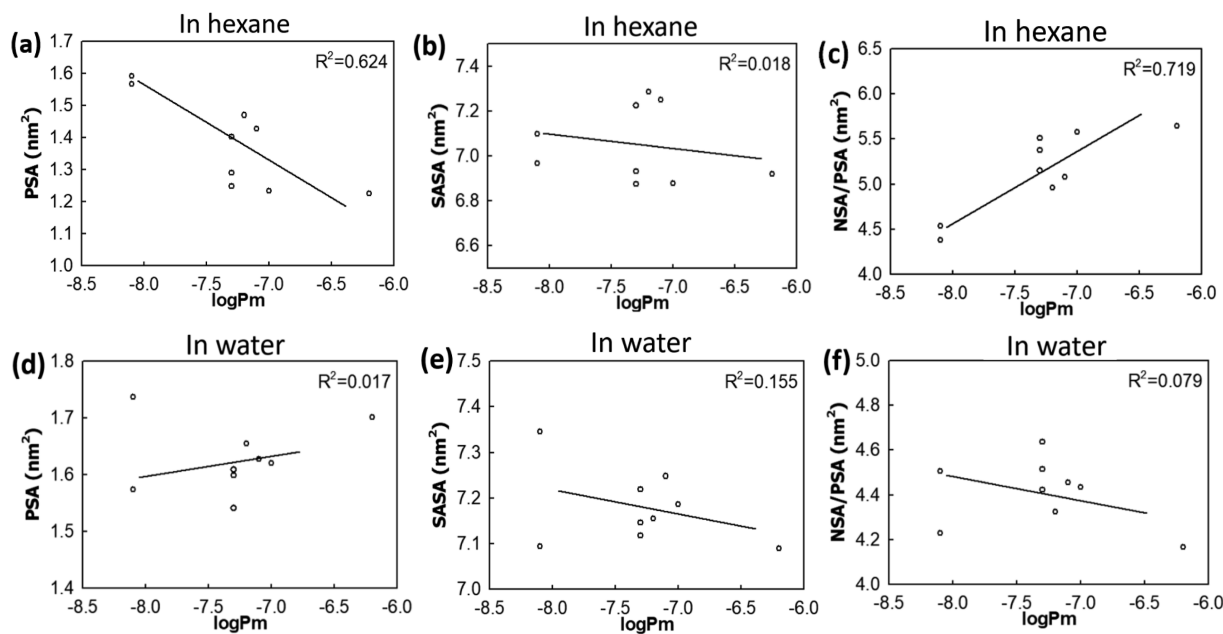


FIG. 2. Correlation of SASA, PSA, and NSA/PSA with the membrane permeability of the cyclic peptides in hexane (a)–(c) and water (d)–(f). The values for the calculated surface parameters are included in Table S3.

The above results suggest that permeability strongly depends on the screening of the polar atoms of these cyclic peptides in hexane. As the polar atoms are mainly part of the peptide backbone (the only other polar atoms are from a Tyr sidechain hydroxyl group), the free energy penalty is largely determined by the desolvation of the backbone polar atoms, which consist of the polar amide NH groups and the polar carbonyl CO groups. To evaluate the relative contributions of NH and CO groups to the overall PSA, we calculated the atomic PSA for the two functional groups NH and CO (Fig. 4). Compared to the CO groups, the accessible atomic area for NH groups is quite low, suggesting that the PSA is largely made up of contributions of the CO groups of the peptide. Indeed, the PSA and cPSA for the CO group show enhanced correlation with permeability, with $R^2 = 0.83$ and 0.827 , respectively [Figs. 4(b) and 4(e)]. The dominance of CO in PSA largely arises from the higher partial charges of the carbon and oxygen atoms, which in turn requires paying larger free energy penalties as they enter the membrane. Further decomposition of the PSA into contributions from each element revealed that O shows the highest correlation with peptide permeability (Fig. S5), as a result of having the highest partial charge.

Compared to small molecules, peptides are flexible and can form a large number of intra-peptide HBs and intermolecular HBs with water (and perhaps inter-peptide HBs depending on the local concentrations of the peptides). The formation of intra-peptide HBs reduces the PSA in the membrane and stabilizes the polar atoms and thus favors membrane translocation, as has been hypothesized for cyclosporine A (CSA).¹⁰ In water, the cyclic peptide CSA adopts an open conformation, with backbone atoms engaged in HBs with water molecules, while in a membrane, CSA adopts a closed conformation driven by the formation of intra-peptide hydrogen

bonds.^{19,63} Thus, the reduction of PSA and the formation of higher number of intra-molecular HBs in the membrane compared to those in water are reasonable indicators of the permeability of the cyclic peptides. However, the changes in total SASA are poorly correlated with peptide permeability (Fig. S6a), but the change in PSA correlates well with permeability (Fig. S6b). When the PSA is reweighted by the atomic charges, the correlation increases slightly (R^2 increases from 0.681 to 0.701 , Fig. S6c). Figure S7 shows that all the cyclic peptides form more intra-peptide hydrogen bonds in hexane than in water, suggesting that the cyclic peptide undergoes a conformational transition when translocating from the aqueous to the membrane phase. Although the number of intra-peptide HBs in water is poorly correlated with membrane permeability, the number of HBs in hexane and the difference in HBs between hexane and water do show some correlation, with R^2 value of 0.410 and 0.336 , respectively.

For most molecules containing polar groups, the main free energy barrier along the translocation pathway lies in the lipid tail region of the membrane.^{16,59,64} The above simulations were performed in hexane, which was selected to mimic the lipid tail region of the membrane. Different organic media have been used in the literature to mimic membranes.⁶⁵ We also performed MD simulations to explore the potential of using chloroform and octanol as membrane mimics, and the corresponding surface areas are shown Figs. S8 and S9. All the descriptors examined above show reduced correlations with peptide permeability in chloroform, and we suspect it results from the small and spherical shape of a chloroform molecule, which is structurally quite different from the extended shapes of the lipid tails of the membrane. In octanol, all descriptors show very poor correlation with peptide permeability (all R^2 values are below 0.15). Due to the presence of the polar hydroxyl

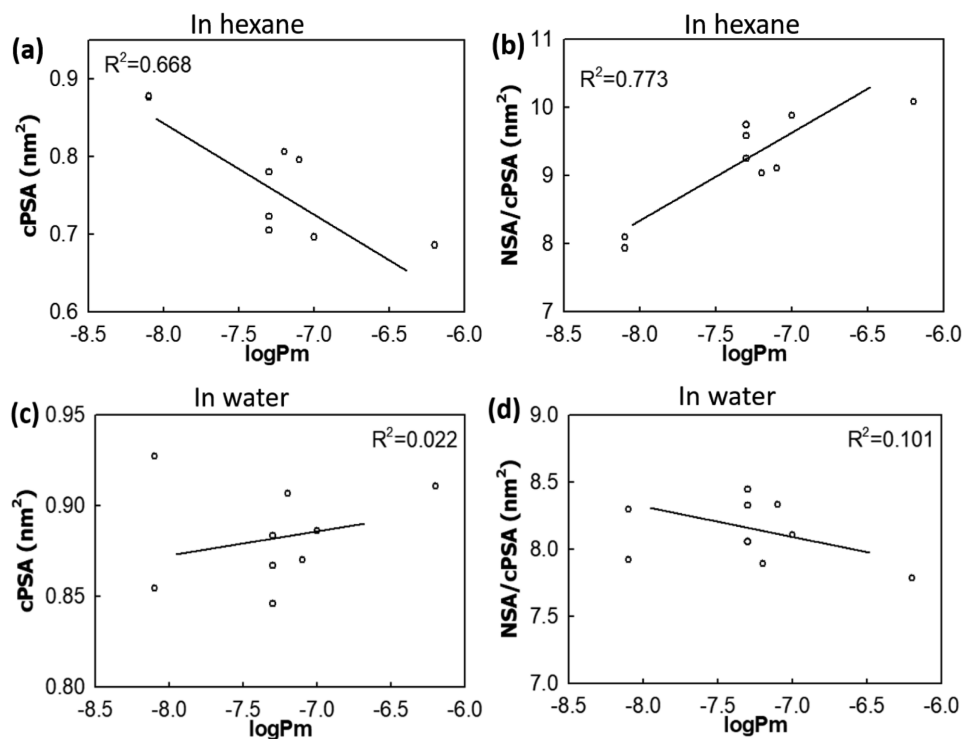


FIG. 3. Correlation of cPSA and NSA/cPSA with the membrane permeability of the cyclic peptides in hexane (a) and (b) and water (c) and (d). For comparison, the calculated parameters for six new crosslinked peptides are also included in (a) and (b). The values for the calculated surface parameters are included in Table S4.

group, octanol is less hydrophobic and has an amphiphilic structure. Together the data suggests that hexane is a better mimic of the lipid tail of the membrane and could arise from its structural similarity with the lipid tails, at least for the set of cyclic peptides explored in this study.

An additional uncertainty in computational predictions of membrane permeability is the choice of force field. There appears to be no general force field that can unambiguously be applied to any given molecule. We decided to explore the use of AMBER03 (we tested this force field because it yielded a good correlation in a study published by Ono *et al.*²⁰), CHARMM36, and CHARMM36M force field on our calculations due to their success in describing peptide and protein molecules.⁵⁰ Figure S10 shows that CHARMM36 results in poor correlations between various surface parameters with the peptide permeability. For CHARMM36M, although PSA, cPSA, NSA/PSA, and NSA/cPSA show certain correlations with peptide permeability, but the correlations are not as good as those obtained using the AMBER14SB force field. (R^2 reduced from 0.624 to 0.37 for PSA, 0.667 to 0.331 for cPSA, 0.719 to 0.293 for NSA/PSA, and 0.773 to 0.225 for NSA/cPSA; Fig. S10.) The simulations using the AMBER03 force field demonstrate poor correlations (Fig. S11). AMBER03 was parameterized using a different approach to that used for the other AMBER force fields, and hence its parameters are substantially different.⁶⁶ The results highlight the strong effects of force fields on the properties calculated and hence remain a large source of ambiguity in any blind tests and prediction efforts. For example, the FDA approved cyclic peptide drug cyclosporine A,

due to the presence of a cis peptide bond between residues 2 and 3, is a big challenge for developing a proper force field to characterize its conformational transition from the aqueous phase to the organic phase.¹⁰ The cyclic peptides used in our study contain only six residues; it is likely that the small backbone ring structures may result in certain backbone constraints that are not properly modeled by the standard force fields; there has been some recent progress;^{67,68} clearly more work needs to be done.

The above results suggest good correlations when using AMBER14SB force field and hexane as the membrane mimicking medium. To understand the associated free energy landscape of the cyclic peptides, we further performed PCA analysis. Figure S12 shows the free energy landscape along the first two principle components PC1 and PC2. Interestingly, in general, the peptides with higher membrane permeability (e.g., pep1) appear to display funnel-shaped landscapes, suggesting that the most populated conformations of pep1 in hexane are energetically favorable. In contrast, the fluctuations of the peptides with low membrane permeability (e.g., pep8 and pep9) are characterized by a more frustrated free energy landscape with more metastable states, resulting in lower populations for the energetically favorable conformations of the two peptides in hexane; an exception is pep7, which displays less flexible conformations, but is known to be less permeable.

The translocation of peptides across the membrane is a complex process that depends on the interplay of hydrophobicity, molecular size, intra-peptide hydrogen bonds, polar surface area,

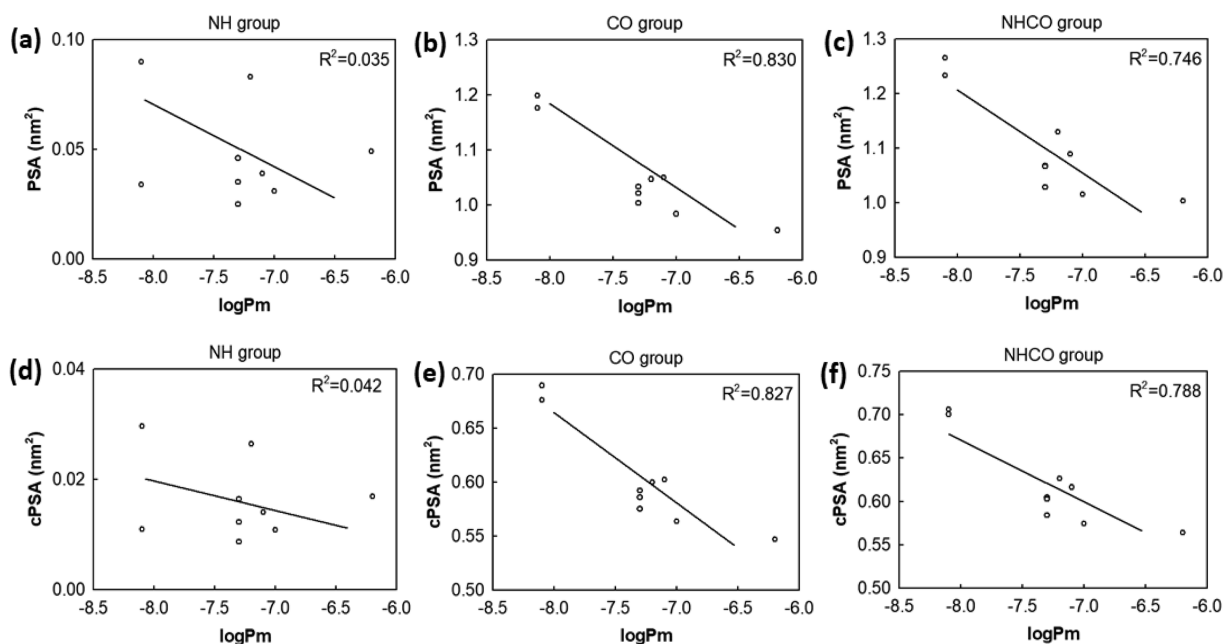


FIG. 4. PSA (a)–(c) and cPSA (d)–(f) of the cyclic peptides in hexane by different functional groups CO, NH, and NHCO. The values for the calculated surface parameters are included in Table S5.

flexibility of the peptide molecule, and the lipid composition of the membrane.^{69–72} For example, the molecular size affects not only the diffusion coefficient but also the free energy cost of a molecule entering the membrane. The larger the molecule, the slower the diffusion and the higher the entropic penalty associated with the creation of a cavity in the membrane to accommodate the molecule.⁷³ Using NMR, Wang *et al.* reported that the experimental diffusion coefficient of a typical six-residue cyclic peptide is in the range of 0.34–0.36 (1×10^{-5} cm²/s), depending on the solvent.⁷⁴ The diffusion coefficient of the cyclic peptides in hexane calculated from our simulations (Table S3) are higher than the reported ones and displays large statistical noise because of the use of only a single peptide in our simulations. Moreover, the RMSD between the peptides used here are small, and yet the computed diffusion coefficients are more widely distributed, pointing to the complex relationship between peptide conformations and their overall mobilities. Hence, it is more appropriate to use the proposed surface parameters as a ranking function for peptides with similar size (e.g., the peptides used in this study). In addition, the membrane permeability of cyclic peptides may also compete with processes, such as (a) the entropic penalties associated with the conformational changes needed for membrane permeation; (b) aggregation that may result from high hydrophobicity and can significantly affect peptide solubility.^{75,76} It is clear that combinations of multiple parameters are required to describe membrane permeability. Naylor *et al.* have used a combination of decadiene–water distribution coefficient and octanol–water partition coefficients to successfully describe the membrane permeability of a set of cyclic peptides, with the former accounting for the tendency to partition into the membrane and the latter

accounting for solubility.⁶⁵ Hence, searching for meaningful parameters can extend the parameter space for peptide permeability. The two new parameters we proposed above, cPSA and NSA/cPSA, can be useful additions to the set of parameters that are combined toward developing multi-variable equations to predict membrane permeability of such molecules. Recently, machine learning methods have been coupled with MD simulations to predict peptide membrane permeability.^{77,78} The new parameters developed in this study can be used as descriptors or molecular features in the machine learning predictions. It is worth noting that the proposed surface parameters are based on an isotropic membrane model, which neglects the inhomogeneity of the membrane as well as the interactions between the peptide and the head groups. Due to such limitations, certain molecular events, such as the peptide conformation at the membrane–water interface, cannot be captured, which has been shown to be important in the translocation of the peptide across the membrane.¹⁶ Atomistic lipid membrane model can be more realistic but are computationally expensive due to the necessity to use enhanced sampling methods, such as replica exchange umbrella sampling simulations.¹⁶ In contrast, the proposed surface parameters (e.g., PSA, cPSA, NSA/PSA) in this study can be easily calculated from a single MD simulation in a membrane mimic media (e.g., hexane) and can be used as *in silico* screens for the rapid identification of potentially membrane permeable peptides, at least for a congeneric series of molecules.

C. Optimization of the peptide scaffold

The findings of our study suggest that the free energy penalty associated with the translocation of the cyclic peptides across the

membrane arises largely from the desolvation of polar backbone atoms, particularly the carbonyl groups. Therefore, we wondered if chemical modifications could be carried out in these peptides to shield the polar backbone atoms, thereby enhancing permeability. As the cyclic peptides have an overall ring structure, a simple strategy may be to link the sidechains of two residues located across the ring, forming a bicyclic peptide in which the linker atoms can shield the backbone polar atoms from one side. Interestingly, romidepsin (ROM), a membrane permeable peptide drug targeting histone deacetylases (HDAC), has a bicyclic structure crosslinked by a disulfide bond⁷⁹ between a Cys residue and an unnatural amino acid that contains an SH group linked to the backbone by a four-carbon chain. Upon entering the cell, the disulfide bond undergoes reduction, resulting in a reduced form of romidepsin (ROH) that binds to histone deacetylases. To examine the effect of the disulfide bond crosslinking on membrane permeability, we simulated ROM and ROH in hexane for 400 ns. Table II shows that ROH has larger PSA and smaller NSA/cPSA values compared to native ROM, suggesting that disulfide crosslinking shields the polar atoms, and it is speculated that this contributes favorably toward the ability of ROM to be membrane permeable.⁸⁰ Based on this speculation, we explore whether similar modifications to our peptides will result in shielding of the polar backbone atoms. We chose two poorly permeable peptides pep8 and pep9 from Table I and mutated the first and fourth Leu residues into two Cys residues linked by a disulfide bridge, yielding two bicyclic peptides pep8cys and pep9cys. These two peptides were subject to MD simulations (for 400 ns) in hexane. The PSA and cPSA of the new peptides were unexpectedly high (Table II), even higher than the parent peptides, suggesting that this modification resulted in a larger exposure of the polar backbone atoms. Visual inspection of the peptide conformations revealed that the backbone ring structures of pep8cys and pep9cys are significantly twisted and likely result from the constraints imposed by the short disulfide linker between the two Cys residues, as shown by the snapshots of the crosslinked peptides in Fig. S13. This was not seen for ROM because the crosslinking chain is much longer and the ring is smaller (five residues compared to six residues in pep8 and pep9). To overcome this, we decided to introduce a longer hydrocarbon cross-linker, and for this, we modeled a staple linker; this technique of stapling is increasingly being used to constrain linear (mostly alpha helical) peptides toward their development as potential therapeutics.^{81,82} We introduced staples across positions 1 and 4 in the parent peptides pep8 and pep9. Two types of staples were introduced: one containing 11 carbon atoms and the other containing 8 carbon atoms, resulting in four stapled cyclic peptides, referred to as pep8s1, pep9s1, pep8s2, and pep9s2 (Table II and Fig. S13). Each stapled cyclic peptide was subjected to 400 ns simulations in hexane. The calculated PSA, cPSA for all the stapled cyclic peptides, are significantly reduced compared to their parent peptides. In particular, the PSA for pep8s1 and pep9s1 are 1.27 and 1.20 nm², respectively, which are similar to the most permeable peptide (e.g., pep1 with PSA 1.23). The peptides with the longer staple (pep8s1 and pep9s1) display much lower PSA than the peptides with a short staple chain (pep8s2 and pep9s2) because the longer staple chains shield larger polar surface areas than the shorter ones. In addition, in hexane (the membrane mimic), the stapled cyclic peptides also form a larger number of intramolecular hydrogen bonds compared to the parent peptides, and this likely favors membrane translocation

(Table II). In contrast, the hydrogen bonds between the peptide and water display no correlation. To further validate the role of hydrocarbon crosslinking in modulating peptide permeability, we used the same hydrocarbon stapling strategy to modify ROM and made two ROM analogs, ROMs1 with a long hydrocarbon chain and ROMs2 with a short chain. We also constructed another romidepsin analog with a longer crosslinking chain, ROM1M, with one additional carbon inserted between the two sulfur atoms. Table II shows that although there is no reduction in PSA for ROM1M, the hydrocarbon crosslinked peptides, ROMs1 and ROMs2, display a reduced PSA and increase in NSA/cPSA compared to the parent peptide ROM; the longer hydrocarbon chain exerts a greater shielding effect on account of the long and flexible hydrocarbon chain. Of course, these last three examples are used here to support our hypothesis of backbone shielding only; since the ROM is thought to function by chelating a zinc in HDAC enzymes through its Cys sulfur,⁸³ these three ROM analogs are expected to be dysfunctional. We also carried out simulations of the peptides in water and calculated the differences in the surface parameters between hexane and water, such as Δ PSA, Δ cPSA, and Δ NSA/cPSA. However, these parameters do not show clear pattern between the parent peptides and the crosslinked peptides.

One may argue that the increase in NSA/PSA and NSA/cPSA may simply result from the larger molecular size arising from the incorporation of the bulky staple chain. To investigate this, we calculated the total surface area and the radius of gyration of the stapled cyclic peptides in hexane and water (Fig. S14). Compared to the parent peptides, the stapled cyclic peptides showed no increase in the radius of gyration and the total surface area in both media. In fact, for pep9s1 and pep9s2, both the total surface area and radius of gyration decrease compared to the parent peptide pep9 even though these two peptides contain larger crosslinkers, suggesting that the two stapled cyclic peptides adopt more compact structures. The results reveal that the hydrocarbon staple chain provides a hydrophobic environment that appears to nucleate the sidechains of other hydrophobic residues into wrapping around the backbone ring, resulting in conformations with more polar backbone atoms buried inside, and suggests a potential way to improve the permeability of cyclic peptides. Clustering the conformations of the peptides sampled during the MD simulations based on their RMSD (Fig. S13) reveals that, for the hydrocarbon crosslinked peptides, the population of the first cluster increases significantly compared to their parent peptides, in both water and hexane, suggesting a reduction in the number of conformational states upon crosslinking. The reduced conformational flexibility of the crosslinked peptides can also be seen from the free energy landscape along the first two principle components (Fig. S15). Compared to the frustrated free energy landscape of the parent peptides pep8 and pep9 (Fig. S12), the crosslinked peptides display more funnel like free energy landscapes (Fig. S15). To understand how the hydrocarbon crosslinking affects the conformational transitions of the stapled cyclic peptides when transferred from water to hexane, we calculated the RMSD of every conformation sampled in water with respect to every conformation sampled in hexane. The distributions of such pairwise RMSD between the two media characterize the similarities between the conformational ensembles of a stapled cyclic peptide between water and hexane. Figure S16 shows that the distribution of RMSD of the crosslinking peptide derivatives shifts to lower

values compared to their parent peptides, suggesting that hydrocarbon crosslinking reduces the differences in conformations between water and hexane. This can reduce the entropic penalties associated with the translocation of the peptide from the aqueous phase to the membrane phase, thus favoring membrane permeation. Therefore, hydrocarbon stapling could be a promising chemical modification to enhance the membrane permeability of peptide drugs. Indeed, stapled alpha-helical peptides have displayed favorable membrane permeability compared to the non-stapled linear peptides,^{84,85} however, hydrocarbon stapling may result in low solubility due to the high hydrophobicity of the hydrocarbon staple chain.

IV. CONCLUDING REMARKS

We have used MD simulations to study the correlation of thermodynamic and structural parameters with the membrane permeability of a set of cyclic peptides that differ from each other only in chirality. MD simulations with realistic lipid membranes are time consuming and often result in the system being trapped in local minima in the complex free energy landscape. This has resulted in the use of organic media to mimic the membrane both experimentally and computationally. We have used three membrane mimicking media, hexane, chloroform, and octanol, and found that hexane was the best at describing the membrane permeability of this set of cyclic peptides. We found that the most widely used parameters in describing the membrane permeability of these cyclic peptides, such as the free energy of transfer between water and the membrane mimicking phase, the ensemble averaged PSA, and the average number of intra-peptide hydrogen bonds, correlate with membrane permeability, with R^2 ranging from 0.41 to 0.624. When the PSA is decomposed into different elements or functional groups, we found an enhanced correlation between the properties of the carbonyl group with peptide permeability. We also proposed two new parameters to determine the ability of peptide to cross membranes: the NSA/PSA ratio, which takes into account both non-polar and polar surface areas, and cPSA, which takes into account the difference in the polarity of the peptide atoms. Both show improved correlations with the membrane permeability of these cyclic peptides, with NSA/cPSA showing the highest correlation, $R^2 = 0.773$. These parameters can easily be obtained from a single simulation of a peptide in hexane. They can also be combined with intra-peptide hydrogen bonds, log P, and other computational and experimental parameters, to provide rapid screening or predictions of the membrane permeability of cyclic peptides. Finally, based on our simulations, we were inspired to introduce hydrocarbon chains to crosslink residues in the cyclic peptides to shield the polar atoms from exposure. These designed peptides showed much reduced PSA and NSA/PSA than their parent peptides, suggesting that these peptides may have higher permeability across membranes, hence opening a new window for the development of cell permeable cyclic stapled peptides as potential peptide therapeutics.

SUPPLEMENTARY MATERIAL

See the [supplementary material](#) for snapshots of the model peptides in hexane and water, surface parameters based on element, surface parameters in octanol and chloroform, surface parameters

using AMBER03 and CHARMM force fields, RMSD, and surface parameters of crosslinked peptides.

ACKNOWLEDGMENTS

The authors would like to acknowledge BMRC/A*STAR ACRC and NSCC for providing the computational resources. This work was supported by collaborative grants from MSD and A*STAR (Grant Nos. H17/01/a0/010, IAF111213C, and SC16/20-302400).

AUTHOR DECLARATIONS

Conflict of Interest

The authors have no conflicts to disclose.

DATA AVAILABILITY

The data that support the findings of this study are available within the article and its [supplementary material](#).

REFERENCES

- 1 A. A. Vinogradov, Y. Yin, and H. Suga, "Macro cyclic peptides as drug candidates: Recent progress and remaining challenges," *J. Am. Chem. Soc.* **141**, 4167–4181 (2019).
- 2 L. K. Buckton, M. N. Rahimi, and S. R. McAlpine, "Cyclic peptides as drugs for intracellular targets: The next frontier in peptide therapeutic development," *Chem. – Eur. J.* **27**, 1487 (2021).
- 3 S. Liras and K. F. McClure, "Permeability of cyclic peptide macrocycles and cyclotides and their potential as therapeutics," *ACS Med. Chem. Lett.* **10**, 1026–1032 (2019).
- 4 H. F. Stähelin, "The history of cyclosporin A (Sandimmune®) revisited: Another point of view," *Experientia* **52**, 5–13 (1996).
- 5 C. Grant, F. Rahman, R. Piekarz, C. Peer, R. Frye, R. W. Robey, E. R. Gardner, W. D. Figg, and S. E. Bates, "Romidepsin: A new therapy for cutaneous T-cell lymphoma and a potential therapy for solid tumors," *Expert Rev. Anticancer Ther.* **10**, 997–1008 (2010).
- 6 R.-J. Lohman, D. S. Nielsen, W. M. Kok, H. N. Hoang, T. A. Hill, and D. P. Fairlie, "Mirror image pairs of cyclic hexapeptides have different oral bioavailabilities and metabolic stabilities," *Chem. Commun.* **55**, 13362–13365 (2019).
- 7 T. Rezai, B. Yu, G. L. Millhauser, M. P. Jacobson, and R. S. Lokey, "Testing the conformational hypothesis of passive membrane permeability using synthetic cyclic peptide diastereomers," *J. Am. Chem. Soc.* **128**, 2510–2511 (2006).
- 8 T. Rezai, J. E. Bock, M. V. Zhou, C. Kalyanaraman, R. S. Lokey, and M. P. Jacobson, "Conformational flexibility, internal hydrogen bonding, and passive membrane permeability: Successful in silico prediction of the relative permeabilities of cyclic peptides," *J. Am. Chem. Soc.* **128**, 14073–14080 (2006).
- 9 P. Ertl, B. Rohde, and P. Selzer, "Fast calculation of molecular polar surface area as a sum of fragment-based contributions and its application to the prediction of drug transport properties," *J. Med. Chem.* **43**, 3714–3717 (2000).
- 10 C. K. Wang, J. E. Swedberg, P. J. Harvey, Q. Kaas, and D. J. Craik, "Conformational flexibility is a determinant of permeability for cyclosporin," *J. Phys. Chem. B* **122**, 2261–2276 (2018).
- 11 S. M. McHugh, J. R. Rogers, H. Yu, and Y.-S. Lin, "Insights into how cyclic peptides switch conformations," *J. Chem. Theory Comput.* **12**, 2480–2488 (2016).
- 12 W. Shinoda, "Permeability across lipid membranes," *Biochim. Biophys. Acta, Biomembr.* **1858**, 2254–2265 (2016).
- 13 R. Sun, Y. Han, J. M. J. Swanson, J. S. Tan, J. P. Rose, and G. A. Voth, "Molecular transport through membranes: Accurate permeability coefficients from multidimensional potentials of mean force and local diffusion constants," *J. Chem. Phys.* **149**, 072310 (2018).
- 14 R. M. Venable, A. Krämer, and R. W. Pastor, "Molecular dynamics simulations of membrane permeability," *Chem. Rev.* **119**, 5954–5997 (2019).

- ¹⁵T. Rivel, C. Ramseyer, and S. Yesylevskyy, "The asymmetry of plasma membranes and their cholesterol content influence the uptake of cisplatin," *Sci. Rep.* **9**, 5627 (2019).
- ¹⁶M. Sugita, S. Sugiyama, T. Fujie, Y. Yoshikawa, K. Yanagisawa, M. Ohue, and Y. Akiyama, "Large-scale membrane permeability prediction of cyclic peptides crossing a lipid bilayer based on enhanced sampling molecular dynamics simulations," *J. Chem. Inf. Model.* **61**, 3681–3695 (2021).
- ¹⁷C. T. Lee, J. Comer, C. Herndon, N. Leung, A. Pavlova, R. V. Swift, C. Tung, C. N. Rowley, R. E. Amaro, C. Chipot, Y. Wang, and J. C. Gumbart, "Simulation-based approaches for determining membrane permeability of small compounds," *J. Chem. Inf. Model.* **56**, 721–733 (2016).
- ¹⁸C. J. Dickson, V. Hornak, D. Bednarczyk, and J. S. Duca, "Using membrane partitioning simulations to predict permeability of forty-nine drug-like molecules," *J. Chem. Inf. Model.* **59**, 236–244 (2019).
- ¹⁹J. Witek, B. G. Keller, M. Blatter, A. Meissner, T. Wagner, and S. Riniker, "Kinetic models of cyclosporin A in polar and apolar environments reveal multiple congruent conformational states," *J. Chem. Inf. Model.* **56**, 1547–1562 (2016).
- ²⁰S. Ono, M. R. Naylor, C. E. Townsend, C. Okumura, O. Okada, and R. S. Lokey, "Conformation and permeability: Cyclic hexapeptide diastereomers," *J. Chem. Inf. Model.* **59**, 2952–2963 (2019).
- ²¹A. S. Kamenik, J. Kraml, F. Hofer, F. Waibl, P. K. Quoika, U. Kahler, M. Schauperl, and K. R. Liedl, "Macrocycle cell permeability measured by solvation free energies in polar and apolar environments," *J. Chem. Inf. Model.* **60**, 3508–3517 (2020).
- ²²P. Stenberg, K. Luthman, and P. Artursson, "Prediction of membrane permeability to peptides from calculated dynamic molecular surface properties," *Pharm. Res.* **16**, 205–212 (1999).
- ²³H. H. F. Refsgaard, B. F. Jensen, P. B. Brockhoff, S. B. Padkjær, M. Guldbbrandt, and M. S. Christensen, "In silico prediction of membrane permeability from calculated molecular parameters," *J. Med. Chem.* **48**, 805–811 (2005).
- ²⁴T. Hou, J. Wang, W. Zhang, W. Wang, and X. Xu, "Recent advances in computational prediction of drug absorption and permeability in drug discovery," *Curr. Med. Chem.* **13**, 2653–2667 (2006).
- ²⁵M. Rossi Sebastian, B. C. Doak, M. Backlund, V. Poongavanam, B. Over, G. Ermondi, G. Caron, P. Matsson, and J. Kihlberg, "Impact of dynamically exposed polarity on permeability and solubility of chameleonic drugs beyond the rule of 5," *J. Med. Chem.* **61**, 4189–4202 (2018).
- ²⁶A. Whitty, M. Zhong, L. Viarengo, D. Beglov, D. R. Hall, and S. Vajda, "Quantifying the chameleonic properties of macrocycles and other high-molecular-weight drugs," *Drug Discovery Today* **21**, 712–717 (2016).
- ²⁷D. F. Veber, S. R. Johnson, H.-Y. Cheng, B. R. Smith, K. W. Ward, and K. D. Kopple, "Molecular properties that influence the oral bioavailability of drug candidates," *J. Med. Chem.* **45**, 2615–2623 (2002).
- ²⁸V. Poongavanam, Y. Atilaw, S. Ye, L. H. E. Wieske, M. Erdelyi, G. Ermondi, G. Caron, and J. Kihlberg, "Predicting the permeability of macrocycles from conformational sampling—Limitations of molecular flexibility," *J. Pharm. Sci.* **110**, 301–313 (2019).
- ²⁹M. Kansy, F. Senner, and K. Gubernator, "Physicochemical high throughput screening: Parallel artificial membrane permeation assay in the description of passive absorption processes," *J. Med. Chem.* **41**, 1007–1010 (1998).
- ³⁰P. Berben, A. Bauer-Brandl, M. Brandl, B. Faller, G. E. Flaten, A.-C. Jacobsen, J. Brouwers, and P. Augustijns, "Drug permeability profiling using cell-free permeation tools: Overview and applications," *Eur. J. Pharm. Sci.* **119**, 219–233 (2018).
- ³¹P. Palumbo, U. Picchini, B. Beck, J. van Gelder, N. Delbar, and A. DeGae-tano, "A general approach to the apparent permeability index," *J. Pharmacokinet. Pharmacodyn.* **35**, 235 (2008).
- ³²C. Tian, K. Kasavajhala, K. A. A. Belfon, L. Raguette, H. Huang, A. N. Miguez, J. Bickel, Y. Wang, J. Pincay, Q. Wu, and C. Simmerling, "ff19SB: Amino-acid-specific protein backbone parameters trained against quantum mechanics energy surfaces in solution," *J. Chem. Theory Comput.* **16**, 528–552 (2020).
- ³³C. Païsonni, F. Nardelli, S. Zanella, F. Curnis, L. Belvisi, G. Musco, and M. Ghitti, "A critical assessment of force field accuracy against NMR data for cyclic peptides containing β -amino acids," *Phys. Chem. Chem. Phys.* **20**, 15807–15816 (2018).
- ³⁴S. Kannan, P. G. A. Aronica, S. Ng, D. T. Gek Lian, Y. Frosi, S. Chee, J. Shimin, T. Y. Yuen, A. Sadruddin, H. Y. K. Kaan, A. Chandramohan, J. H. Wong, Y. S. Tan, Z. W. Chang, F. J. Ferrer-Gago, P. Arumugam, Y. Han, S. Chen, L. Rénia, C. J. Brown, C. W. Johannes, B. Henry, D. P. Lane, T. K. Sawyer, C. S. Verma, and A. W. Partridge, "Macrocyclization of an all-D linear α -helical peptide imparts cellular permeability," *Chem. Sci.* **11**, 5577–5591 (2020).
- ³⁵C. I. Bayly, P. Cieplak, W. Cornell, and P. A. Kollman, "A well-behaved electrostatic potential based method using charge restraints for deriving atomic charges: The RESP model," *J. Phys. Chem.* **97**, 10269–10280 (1993).
- ³⁶P. Cieplak, W. D. Cornell, C. Bayly, and P. A. Kollman, "Application of the multimolecule and multiconformational RESP methodology to biopolymers: Charge derivation for DNA, RNA, and proteins," *J. Comput. Chem.* **16**, 1357–1377 (1995).
- ³⁷M. Valiev, E. J. Bylaska, N. Govind, K. Kowalski, T. P. Straatsma, H. J. J. Van Dam, D. Wang, J. Nieplocha, E. Apra, T. L. Windus, and W. A. de Jong, "NWChem: A comprehensive and scalable open-source solution for large scale molecular simulations," *Comput. Phys. Commun.* **181**, 1477–1489 (2010).
- ³⁸F.-Y. Dupradeau, A. Pigache, T. Zaffran, C. Savineau, R. Lelong, N. Grivel, D. Lelong, W. Rosanski, and P. Cieplak, "The R.E.D. tools: Advances in RESP and ESP charge derivation and force field library building," *Phys. Chem. Chem. Phys.* **12**, 7821–7839 (2010).
- ³⁹R. Salomon-Ferrer, D. A. Case, and R. C. Walker, "An overview of the Amber biomolecular simulation package," *Wiley Interdiscip. Rev.: Comput. Mol. Sci.* **3**, 198–210 (2013).
- ⁴⁰J. Wang, W. Wang, P. A. Kollman, and D. A. Case, "Automatic atom type and bond type perception in molecular mechanical calculations," *J. Mol. Graphics Modell.* **25**, 247–260 (2006).
- ⁴¹J. A. Maier, C. Martinez, K. Kasavajhala, L. Wickstrom, K. E. Hauser, and C. Simmerling, "ff14SB: Improving the accuracy of protein side chain and backbone parameters from ff99SB," *J. Chem. Theory Comput.* **11**, 3696–3713 (2015).
- ⁴²W. L. Jorgensen, J. Chandrasekhar, J. D. Madura, R. W. Impey, and M. L. Klein, "Comparison of simple potential functions for simulating liquid water," *J. Chem. Phys.* **79**, 926–935 (1983).
- ⁴³D. van der Spoel, M. M. Ghahremanpour, and J. A. Lemkul, "Small molecule thermochemistry: A tool for empirical force field development," *J. Phys. Chem. A* **122**, 8982–8988 (2018).
- ⁴⁴J. Yoo and Q. Cui, "Does arginine remain protonated in the lipid membrane? Insights from microscopic pK_a calculations," *Biophys. J.* **94**, L61–L63 (2008).
- ⁴⁵T.-L. Sun and H. W. Huang, "Membrane permeability of peptides and drugs," *Biophys. J.* **104**, 599a (2013).
- ⁴⁶T. Wymore and T. C. Wong, "Molecular dynamics study of substance P peptides in a biphasic membrane mimic," *Biophys. J.* **76**, 1199–1212 (1999).
- ⁴⁷S. Kumar, J. M. Rosenberg, D. Bouzida, R. H. Swendsen, and P. A. Kollman, "The weighted histogram analysis method for free-energy calculations on biomolecules. I. The method," *J. Comput. Chem.* **13**, 1011–1021 (1992).
- ⁴⁸F. Eisenhaber, P. Lijnzaad, P. Argos, C. Sander, and M. Scharf, "The double cubic lattice method: Efficient approaches to numerical integration of surface area and volume and to dot surface contouring of molecular assemblies," *J. Comput. Chem.* **16**, 273–284 (1995).
- ⁴⁹B. Lee and F. M. Richards, "The interpretation of protein structures: Estimation of static accessibility," *J. Mol. Biol.* **55**, 379 (1971).
- ⁵⁰R. B. Best, X. Zhu, J. Shim, P. E. M. Lopes, J. Mittal, M. Feig, and A. D. MacKerell, "Optimization of the additive CHARMM all-atom protein force field targeting improved sampling of the backbone ϕ , ψ and side-chain $\chi(1)$ and $\chi(2)$ dihedral angles," *J. Chem. Theory Comput.* **8**, 3257–3273 (2012).
- ⁵¹J. Huang, S. Rauscher, G. Nawrocki, T. Ran, M. Feig, B. L. de Groot, H. Grubmüller, and A. D. MacKerell, Jr., "CHARMM36m: An improved force field for folded and intrinsically disordered proteins," *Nat. Methods* **14**, 71–73 (2017).
- ⁵²J. Lee, X. Cheng, J. M. Swails, M. S. Yeom, P. K. Eastman, J. A. Lemkul, S. Wei, J. Buckner, J. C. Jeong, Y. Qi, S. Jo, V. S. Pande, D. A. Case, C. L. Brooks, A. D. MacKerell, J. B. Klauda, and W. Im, "CHARMM-GUI input generator for NAMD, GROMACS, AMBER, OpenMM, and CHARMM/OpenMM simulations using the CHARMM36 additive force field," *J. Chem. Theory Comput.* **12**, 405–413 (2016).
- ⁵³S. Jo, T. Kim, V. G. Iyer, and W. Im, "CHARMM-GUI: A web-based graphical user interface for CHARMM," *J. Comput. Chem.* **29**, 1859–1865 (2008).
- ⁵⁴Y. Duan, C. Wu, S. Chowdhury, M. C. Lee, G. Xiong, W. Zhang, R. Yang, P. Cieplak, R. Luo, T. Lee, J. Caldwell, J. Wang, and P. Kollman, "A point-charge

- force field for molecular mechanics simulations of proteins based on condensed-phase quantum mechanical calculations,” *J. Comput. Chem.* **24**, 1999–2012 (2003).
- ⁵⁵B. Hess, H. Bekker, H. J. C. Berendsen, and J. G. E. M. Fraaije, “LINCS: A linear constraint solver for molecular simulations,” *J. Comput. Chem.* **18**, 1463–1472 (1997).
- ⁵⁶U. Essmann, L. Perera, M. L. Berkowitz, T. Darden, H. Lee, and L. G. Pedersen, “A smooth particle mesh Ewald method,” *J. Chem. Phys.* **103**, 8577–8593 (1995).
- ⁵⁷P. Bjelkmar, P. Larsson, M. A. Cuendet, B. Hess, and E. Lindahl, “Implementation of the CHARMM force field in GROMACS: Analysis of protein stability effects from correction maps, virtual interaction sites, and water models,” *J. Chem. Theory Comput.* **6**, 459–466 (2010).
- ⁵⁸J. L. MacCallum, W. F. D. Bennett, and D. P. Tieleman, “Distribution of amino acids in a lipid bilayer from computer simulations,” *Biophys. J.* **94**, 3393–3404 (2008).
- ⁵⁹J. Li, R. W. Beuerman, and C. S. Verma, “Molecular insights into the membrane affinities of model hydrophobes,” *ACS Omega* **3**, 2498–2507 (2018).
- ⁶⁰J. Marrero and R. Gani, “Group contribution-based estimation of octanol/water partition coefficient and aqueous solubility,” *Ind. Eng. Chem. Res.* **41**, 6623–6633 (2002).
- ⁶¹K. Chen, Y. Sheng, J. Wang, and W. Wang, “Chirality-dependent adsorption between amphipathic peptide and POPC membrane,” *Int. J. Mol. Sci.* **20**, 4760 (2019).
- ⁶²P. Arranz-Gibert, B. Guixer, M. Malakoutikhah, M. Muttenthaler, F. Guzmán, M. Teixidó, and E. Giralt, “Lipid bilayer crossing—The gate of symmetry. Water-soluble phenylproline-based blood-brain barrier shuttles,” *J. Am. Chem. Soc.* **137**, 7357–7364 (2015).
- ⁶³J. Witek, S. Wang, B. Schroeder, R. Lingwood, A. Dounas, H.-J. Roth, M. Fouché, M. Blatter, O. Lemke, B. Keller, and S. Riniker, “Rationalization of the membrane permeability differences in a series of analogue cyclic decapeptides,” *J. Chem. Inf. Model.* **59**, 294–308 (2019).
- ⁶⁴S. Yesylevskyy, S.-J. Marrink, and A. E. Mark, “Alternative mechanisms for the interaction of the cell-penetrating peptides penetratin and the TAT peptide with lipid bilayers,” *Biophys. J.* **97**, 40–49 (2009).
- ⁶⁵M. R. Naylor, A. M. Ly, M. J. Handford, D. P. Ramos, C. R. Pye, A. Furukawa, V. G. Klein, R. P. Noland, Q. Edmondson, A. C. Turmon, W. M. Hewitt, J. Schwochert, C. E. Townsend, C. N. Kelly, M.-J. Blanco, and R. S. Lokey, “Lipophilic permeability efficiency reconciles the opposing roles of lipophilicity in membrane permeability and aqueous solubility,” *J. Med. Chem.* **61**, 11169–11182 (2018).
- ⁶⁶V. Hornak, R. Abel, A. Okur, B. Strockbine, A. Roitberg, and C. Simmerling, “Comparison of multiple Amber force fields and development of improved protein backbone parameters,” *Proteins: Struct., Funct., Bioinf.* **65**, 712–725 (2006).
- ⁶⁷H. Geng, F. Jiang, and Y.-D. Wu, “Accurate structure prediction and conformational analysis of cyclic peptides with residue-specific force fields,” *J. Phys. Chem. Lett.* **7**, 1805–1810 (2016).
- ⁶⁸D. P. Slough, H. Yu, S. M. McHugh, and Y.-S. Lin, “Toward accurately modeling N-methylated cyclic peptides,” *Phys. Chem. Chem. Phys.* **19**, 5377–5388 (2017).
- ⁶⁹P. Mattsson and J. Kihlberg, “How big is too big for cell permeability?” *J. Med. Chem.* **60**, 1662–1664 (2017).
- ⁷⁰E. G. Chikhale, K. Y. Ng, P. S. Burton, and R. T. Borchardt, “Hydrogen bonding potential as a determinant of the *in vitro* and *in situ* blood–brain barrier permeability of peptides,” *Pharm. Res.* **11**, 412–419 (1994).
- ⁷¹P. G. Dougherty, A. Sahni, and D. Pei, “Understanding cell penetration of cyclic peptides,” *Chem. Rev.* **119**, 10241–10287 (2019).
- ⁷²Z. Cao, X. Zhang, C. Wang, L. Liu, L. Zhao, J. Wang, and Y. Zhou, “Different effects of cholesterol on membrane permeation of arginine and tryptophan revealed by bias-exchange metadynamics simulations,” *J. Chem. Phys.* **150**, 084106 (2019).
- ⁷³S. S. F. Leung, J. Mijalkovic, K. Borrelli, and M. P. Jacobson, “Testing physical models of passive membrane permeation,” *J. Chem. Inf. Model.* **52**, 1621–1636 (2012).
- ⁷⁴C. K. Wang, S. E. Northfield, J. E. Swedberg, P. J. Harvey, A. M. Mathiowitz, D. A. Price, S. Liras, and D. J. Craik, “Translational diffusion of cyclic peptides measured using pulsed-field gradient NMR,” *J. Phys. Chem. B* **118**, 11129–11136 (2014).
- ⁷⁵D. S. Nielsen, R.-J. Lohman, H. N. Hoang, T. A. Hill, A. Jones, A. J. Lucke, and D. P. Fairlie, “Flexibility versus rigidity for orally bioavailable cyclic hexapeptides,” *ChemBioChem* **16**, 2289–2293 (2015).
- ⁷⁶J. Schwochert, Y. Lao, C. R. Pye, M. R. Naylor, P. V. Desai, I. C. Gonzalez Valcarcel, J. A. Barrett, G. Sawada, M.-J. Blanco, and R. S. Lokey, “Stereocchemistry balances cell permeability and solubility in the naturally derived phepropeptin cyclic peptides,” *ACS Med. Chem. Lett.* **7**, 757–761 (2016).
- ⁷⁷E. C. L. de Oliveira, K. Santana, L. Josino, A. H. Lima e Lima, and C. de Souza de Sales Júnior, “Predicting cell-penetrating peptides using machine learning algorithms and navigating in their chemical space,” *Sci. Rep.* **11**, 7628 (2021).
- ⁷⁸D. P. Tran, S. Tada, A. Yumoto, A. Kitao, Y. Ito, T. Uzawa, and K. Tsuda, “Using molecular dynamics simulations to prioritize and understand AI-generated cell penetrating peptides,” *Sci. Rep.* **11**, 10630 (2021).
- ⁷⁹H. Nakajima, Y. B. Kim, H. Terano, M. Yoshida, and S. Horinouchi, “FR901228, a potent antitumor antibiotic, is a novel histone deacetylase inhibitor,” *Exp. Cell Res.* **241**, 126–133 (1998).
- ⁸⁰J. Li, C. Wang, Z.-M. Zhang, Y.-Q. Cheng, and J. Zhou, “The structural basis of an NADP⁺-independent dithiol oxidase in FK228 biosynthesis,” *Sci. Rep.* **4**, 4145 (2014).
- ⁸¹L. D. Walensky and G. H. Bird, “Hydrocarbon-stapled peptides: Principles, practice, and progress,” *J. Med. Chem.* **57**, 6275–6288 (2014).
- ⁸²C. E. Schafmeister, J. Po, and G. L. Verdine, “An all-hydrocarbon cross-linking system for enhancing the helicity and metabolic stability of peptides,” *J. Am. Chem. Soc.* **122**, 5891–5892 (2000).
- ⁸³B. C. Valdez, J. E. Brammer, Y. Li, D. Murray, Y. Liu, C. Hosing, Y. Nieto, R. E. Champlin, and B. S. Andersson, “Romidepsin targets multiple survival signaling pathways in malignant T cells,” *Blood Cancer J.* **5**, e357 (2015).
- ⁸⁴Q. Chu, R. E. Moellering, G. J. Hilinski, Y.-W. Kim, T. N. Grossmann, J. T.-H. Yeh, and G. L. Verdine, “Towards understanding cell penetration by stapled peptides,” *MedChemComm* **6**, 111–119 (2015).
- ⁸⁵T.-L. Sun, Y. Sun, C.-C. Lee, and H. W. Huang, “Membrane permeability of hydrocarbon-cross-linked peptides,” *Biophys. J.* **104**, 1923–1932 (2013).